

Platinum-Based Chemotherapy Induces Opposing Effects on Immunotherapy Response-Related Spatial and Stromal Biomarkers in the Bladder Cancer Microenvironment

Chelushkin, Maksim A.; van Dorp, Jeroen; van Wilpe, Sandra; Seignette, Iris M.; Gil-Jimenez, Alberto; Peters, Dennis; Hooijberg, Erik; van der Heijden, Antoine G.; Wessels, Lodewyk F.A.; More Authors

DOI

[10.1158/1078-0432.CCR-24-0724](https://doi.org/10.1158/1078-0432.CCR-24-0724)

Publication date

2024

Document Version

Final published version

Published in

Clinical cancer research : an official journal of the American Association for Cancer Research

Citation (APA)

Chelushkin, M. A., van Dorp, J., van Wilpe, S., Seignette, I. M., Gil-Jimenez, A., Peters, D., Hooijberg, E., van der Heijden, A. G., Wessels, L. F. A., & More Authors (2024). Platinum-Based Chemotherapy Induces Opposing Effects on Immunotherapy Response-Related Spatial and Stromal Biomarkers in the Bladder Cancer Microenvironment. *Clinical cancer research : an official journal of the American Association for Cancer Research*, 30(18), 4227-4239. <https://doi.org/10.1158/1078-0432.CCR-24-0724>

Important note

To cite this publication, please use the final published version (if applicable).
Please check the document version above.

Copyright

Other than for strictly personal use, it is not permitted to download, forward or distribute the text or part of it, without the consent of the author(s) and/or copyright holder(s), unless the work is under an open content license such as Creative Commons.

Takedown policy

Please contact us and provide details if you believe this document breaches copyrights.
We will remove access to the work immediately and investigate your claim.

Green Open Access added to TU Delft Institutional Repository

'You share, we take care!' - Taverne project

<https://www.openaccess.nl/en/you-share-we-take-care>

Otherwise as indicated in the copyright section: the publisher is the copyright holder of this work and the author uses the Dutch legislation to make this work public.



Platinum-Based Chemotherapy Induces Opposing Effects on Immunotherapy Response-Related Spatial and Stromal Biomarkers in the Bladder Cancer Microenvironment

Maksim A. Chelushkin^{1,2,3}, Jeroen van Dorp^{1,4}, Sandra van Wilpe⁵, Iris M. Seignette⁶, Jan-Jaap J. Mellema^{1,4}, Maartje Alkemade⁷, Alberto Gil-Jimenez^{1,3}, Dennis Peters⁷, Wim Brugman⁸, Chantal F. Stockem^{1,4}, Erik Hooijberg⁶, Annegien Broeks⁷, Bas W.G. van Rhijn^{9,10}, Laura S. Mertens⁹, Antoine G. van der Heijden¹¹, Niven Mehra⁵, Maurits L. van Montfoort⁶, Lodewyk F.A. Wessels^{1,3,12}, Daniel J. Vis^{1,3}, and Michiel S. van der Heijden^{1,4}

ABSTRACT

Purpose: Platinum-based chemotherapy and immune checkpoint inhibitors are key components of systemic treatment for muscle-invasive and advanced urothelial cancer. The ideal integration of these two treatment modalities remains unclear as clinical trials have led to inconsistent results. Modulation of the tumor-immune microenvironment by chemotherapy is poorly characterized. We aimed to investigate this modulation, focusing on potential clinical implications for immune checkpoint inhibitor response.

Experimental Design: We assessed immune cell densities, spatial relations, and tumor/stromal components from 116 patients with urothelial bladder cancer (paired data for 95 patients) before and after platinum-based chemotherapy.

Results: Several published biomarkers for immunotherapy response changed upon chemotherapy treatment. The intratumoral CD8⁺ T-cell percentage increased after treatment and was associated with increased TNF α -via-NF- κ B signaling. The percentage of

PDL1⁺ immune cells was higher after chemotherapy. An increase in chemo-induced changes that potentially inhibit an antitumor immune response was also observed, including increased fibroblast-based TGF β signaling and distances from immune cells to the nearest cancer cell. The latter two parameters correlated significantly in posttreatment samples, suggesting that TGF β signaling in fibroblasts may play a role in spatially separating immune cells from cancer cells. We examined specific chemotherapy regimens and found that treatment with methotrexate, vinblastine, doxorubicin, and cisplatin was associated with an increase in the macrophage cell percentage. Gemcitabine-containing chemotherapy was associated with upregulation of fibroblast TGF β signaling.

Conclusions: The opposing effects of platinum-based chemotherapy on the immune cell composition and stromal context of the tumor-immune microenvironment may explain the inconsistent results of clinical trials investigating chemotherapy and immune checkpoint inhibitor combinations in bladder cancer.

Introduction

Cisplatin-based neoadjuvant chemotherapy (NAC) followed by radical cystectomy is recommended for patients with muscle-invasive bladder cancer (MIBC; ref. 1). Accelerated methotrexate, vinblastine, doxorubicin, and cisplatin (MVAC) and cisplatin-gemcitabine are the two most commonly used NAC regimens for MIBC (2). Despite a pathological complete response rate (pCR) of 25% to 42%, cisplatin-based NAC is associated with only a 5% to 8% absolute increase in 5-year overall survival (OS) compared with radical cystectomy alone (3–5).

Recently, the CheckMate-274 trial showed that adjuvant treatment with nivolumab (a PD1 inhibitor) significantly increased disease-free survival (DFS) for patients with residual MIBC or lymph node involvement (6). Exploratory analyses revealed a notable improvement in DFS for patients who were previously treated with cisplatin-based NAC [hazard ratio (HR): 0.52; 95% CI, 0.38–0.71 for nivolumab vs. placebo], whereas those who did not receive NAC seemed to have limited benefit (HR: 0.92; 95% CI, 0.69–1.21). In the metastatic setting, improved clinical outcomes have been observed in patients treated with avelumab (anti-PDL1) maintenance therapy after platinum-based chemotherapy, similarly suggesting the benefit of sequential treatment with chemo- and immunotherapy (7).

Clinical trials exploring concurrent chemotherapy and immune checkpoint inhibitors (ICI) have shown mixed results. In the

¹Department of Molecular Carcinogenesis, The Netherlands Cancer Institute, Amsterdam, the Netherlands. ²Department of Tumor Biology and Immunology, The Netherlands Cancer Institute, Amsterdam, the Netherlands. ³OncoCode Institute, Utrecht, the Netherlands. ⁴Department of Medical Oncology, The Netherlands Cancer Institute, Amsterdam, the Netherlands. ⁵Department of Medical Oncology, Radboud University Medical Center, Nijmegen, the Netherlands. ⁶Department of Pathology, Netherlands Cancer Institute, Amsterdam, the Netherlands. ⁷Core Facility Molecular Pathology & Biobanking, Netherlands Cancer Institute, Amsterdam, the Netherlands. ⁸Genomics Core Facility, Netherlands Cancer Institute, Amsterdam, the Netherlands. ⁹Department of Urology, The Netherlands Cancer Institute, Amsterdam, the Netherlands. ¹⁰Department of Urology, Caritas St. Josef Medical Center, University of Regensburg, Regensburg, Germany. ¹¹Department of Urology, Radboud University Medical Center, Nijmegen, the Netherlands. ¹²Faculty of Electrical Engineering, Mathematics and Computer Science, Delft University of Technology, Delft, the Netherlands.

M.A. Chelushkin and J. van Dorp contributed equally to this article.

Corresponding Author: Michiel S. van der Heijden, Netherlands Cancer Institute, Department of Medical Oncology, Department of Molecular Carcinogenesis, Plesmanlaan 121, Amsterdam 1066 CX, the Netherlands. E-mail: ms.vd.heijden@nki.nl

Clin Cancer Res 2024;30:4227–39

doi: 10.1158/1078-0432.CCR-24-0724

©2024 American Association for Cancer Research

Translational Relevance

In various tumor types, successful synergy of chemotherapy and immune checkpoint inhibitors (ICI) has been established, but in muscle-invasive bladder cancer (MIBC), clinical trials yielded inconsistent results. Therefore, understanding chemotherapy-induced changes in the tumor-immune microenvironment (TME) of MIBC is highly relevant. We collected and analyzed a large dataset of paired pre- and post-platinum treatment tumor samples. We demonstrate that platinum-based neoadjuvant chemotherapy (NAC) is associated with an increase in the TME characteristics previously shown to relate to both ICI response and resistance. The latter includes fibroblast-based TGF β signaling and distance from CD8⁺ T cells and macrophages to their nearest cancer cells. This suggests that response to ICI in MIBC after platinum-based NAC might be improved by adding TGF β inhibitors or bispecific antibodies promoting spatial rearrangements of immune and cancer cells. Finally, our data suggest differences between methotrexate, vinblastine, doxorubicin, and cisplatin and gemcitabine-containing platinum-based regimens in their effects on bladder TME.

IMvigor130 trial, atezolizumab combined with platinum-based chemotherapy as first-line treatment for advanced urothelial cancer improved progression-free survival (PFS) compared with chemotherapy alone, although the improvement in OS (final one-sided P value = 0.023) did not reach statistical significance (final OS efficacy boundary: P value = 0.021; refs. 8, 9). In an exploratory analysis, a more pronounced benefit of atezolizumab on OS (and PFS) was observed in the cisplatin-treated subgroup (HR for PFS: 0.73; 95% CI, 0.55–0.97) versus the carboplatin-treated subgroup (HR for PFS: 0.84; 95% CI, 0.70–1.02; ref. 8). The CheckMate-901 study specifically tested the addition of nivolumab to cisplatin-based chemotherapy, reporting positive results for the primary endpoints OS (HR = 0.78) and PFS (HR = 0.72; ref. 10). These findings suggest that the combination of ICI with cisplatin-based chemotherapy are more effective than that with carboplatin-based chemotherapy. Conversely, the addition of pembrolizumab to first-line platinum-based chemotherapy in the KEYNOTE 361 study did not significantly improve PFS or OS by central review in the unselected population per the prespecified P value boundaries (11). However, hazard ratios for PFS were 0.78 (95% CI, 0.65–0.93) in the total population and 0.67 (95% CI, 0.51–0.89) in the choice-of-cisplatin subgroup (11).

Although clinical trials indicate potential synergy between platinum-based chemotherapy and ICI (either sequential or concurrent), results have not been unequivocally positive. Additionally, the positive results may partly be explained by earlier ICI initiation as only a subset of patients (25%–48%) in the standard arms of the chemo-immunotherapy trials in the advanced urothelial cancer setting received ICI as subsequent therapy (7, 8, 10, 11). Given the disappointing results in several trials testing concurrent platinum-based chemotherapy and ICI, particularly when combining carboplatin-based chemotherapy with ICI, a negative interaction between chemotherapy and ICI (e.g., by immune suppression) in a subset of patients cannot be excluded (8, 11).

Here, we investigate changes in the bladder cancer tumor microenvironment (TME) induced by platinum-based NAC, focusing on potential implications for immunotherapy treatment. For this

purpose, we collected and analyzed RNA-sequencing (RNA-seq), multiplex immunofluorescence (mIF), and immunohistochemistry (IHC) data of tumor tissue from patients with MIBC before and after treatment with platinum-based chemotherapy.

Materials and Methods

Patient population

We retrospectively included patients who were treated with neoadjuvant chemotherapy followed by radical cystectomy for MIBC (cT2-4N0-3). Only patients with remaining viable tumor tissue after cystectomy were included (\geq ypT1), regardless of nodal status (Supplementary Fig. S1). Exclusion criteria were prior pelvic radiotherapy and nonurothelial primary histology. Urothelial carcinoma with squamous and/or glandular differentiation was allowed. Patients underwent radical cystectomy between 1995 and 2021. Follow-up was performed according to local guidelines. The retrospective use of biospecimens has been executed pursuant to Dutch legislation and international standards. This non-interventional retrospective study was approved by the NKI institutional review board (IRB; IRBm20-296) and the Radboudumc IRB (2020–6117). All patients signed informed consent and/or participated in the informed opt-out procedure for residual tissue. Within the opt-out framework, patients are informed and have the opportunity to object to the (continued) use of their personal data and biospecimens. This procedure was approved and governed by the NKI IRB, adhering to the CIOMS and other (inter-)national legislative and ethical guidelines.

Tissue collection and RNA isolation

Pretreatment transurethral resection of the bladder tumor (TUR-BT) and posttreatment cystectomy material were stored as formalin-fixed paraffin-embedded (FFPE) tissue blocks in the Netherlands Cancer Institute. Tumor material from patients who had their TUR-BT or cystectomy in a different hospital was requested as tissue blocks and subsequently stored at the Netherlands Cancer Institute.

An experienced uro-pathologist assessed all available tissue blocks, and the most representative tissue block was selected. Tumor area and tumor cell percentage were determined by an experienced uro-pathologist. RNA was isolated from baseline tumor material (5–10 \times 10 μ m slides) using the Qiagen AllPrep FFPE DNA/RNA Kit.

RNA sequencing

The quality and quantity of the total RNA were assessed using the Agilent 2100 Bioanalyzer (RRID:SCR_018043) and a Nano chip (Agilent). The percentage of RNA fragments with >200-nucleotide fragment distribution values (DV200) were determined using the region analysis method according to the manufacturer's instructions (Illumina, technical-note-470-2014-001). Strand-specific libraries were generated using the TruSeq RNA exome library prep kit (Illumina) according to the manufacturer's instructions (Illumina, 1000000039582v01). Briefly, total RNA was random primed and reverse transcribed using SuperScript II reverse transcriptase (Invitrogen, 18064-014) with the addition of actinomycin D. Second strand synthesis was performed using polymerase I and RNaseH with the replacement of dTTP for dUTP. The generated cDNA fragments were 3'-end adenylated and ligated to Illumina (batch 1, 140 samples) or Integrated DNA Technologies xGen UDI(10 bp)-UMI(9 bp; batch 2, 35 samples) paired-end sequencing adapters and subsequently amplified by 15 cycles of PCR. The libraries were

validated on the Agilent 2100 Bioanalyzer (RRID:SCR_018043) using a 7,500 chip followed by a 1 to 4 plex library pooling containing up to 200 ng of each sample. The pooled libraries were enriched for target regions using the probe Coding Exome Oligos set (CEX, 45MB) according to the manufacturer's instruction (Illumina, 1000000039582v01). Briefly, cDNA libraries and biotin-labeled capture probes were combined and hybridized via denaturation at 95°C for 10 minutes and incubation at 94°C to 58°C with a ramp of 18 cycles, with 1-minute incubation and 2°C temperature change per cycle. The hybridized target regions were captured using streptavidin magnetic beads and subjected to two stringency washes, an elution step, and a second round of enrichment followed by cleanup using AMPure XP beads (Beckman, A63881) and PCR amplification of 10 cycles. The target enriched pools were analyzed on the Agilent 2100 Bioanalyzer (RRID:SCR_018043) using a 7,500 chip, diluted, and subsequently pooled equimolar into a multiplex sequencing pool. The libraries from 140 samples originating from 74 patients (batch 1) were sequenced with 65-bp single-end reads on the Illumina HiSeq 2500 System (RRID:SCR_016383) using V4 chemistry. The libraries from an additional 35 samples (from the other 25 patients, batch 2) were sequenced with 54-bp paired-end reads on the Illumina NovaSeq 6000 System (RRID:SCR_016387) using an SP Reagent Kit v1.5 (100 cycles).

Immunohistochemistry and multiplex immunofluorescence

IHC of the FFPE tumor samples was performed on a BenchMark Ultra autostainer [Ventana Medical Systems (RRID:SCR_013652)]. Briefly, paraffin sections were cut at 3 µm, heated at 75°C for 28 minutes, and deparaffinized in the instrument with EZ prep solution (Ventana Medical Systems). Heat-induced antigen retrieval was carried out using cell conditioning 1 (Ventana Medical Systems) for 48 minutes at 95°C. PDL1 was detected using clone 22C3 (Agilent Cat# M365329-2, RRID:AB_2861298; 1/40 dilution, 1 hour at RT, Agilent/DAKO). Bound antibody was detected using the OptiView DAB Detection Kit (Ventana Medical Systems). Slides were counterstained with hematoxylin and bluing reagent (Ventana Medical Systems). A PANNORAMIC 1000 scanner from 3DHIS-TECH was used to scan the slides at a 40× magnification. After scanning, PDL1 and hematoxylin and eosin slides were uploaded to Slide Score (www.slidescore.com) for manual scoring. An experienced uro-pathologist determined the percentage of PDL1 positive tumor cells (TC), percentage of PDL1 positive immune cells (IC), and the combined positivity score (CPS).

Analysis of tumor-immune cell infiltrates anti-CD3 (1:400 dilution clone SP7, Thermo Fisher Scientific Cat# RM-9107-S1, RRID:AB_149924), anti-CD8 (1:100 dilution clone C8/144B, Dako, Agilent Cat# M710301-2, RRID:AB_2075537), anti-CD68 (1:500 dilution clone KP1, Dako, Agilent Cat# M081401-2, RRID:AB_2750584), anti-FoxP3 (1:50 dilution clone 236A/E7, Abcam Cat# ab20034, RRID:AB_445284), anti-CD20 (1:500 dilution clone L26, Dako, Agilent Cat# M075501-2, RRID:AB_2282030), and anti-PanCK (1:100 dilution clone AE1/AE3, Abcam Cat# ab27988, RRID:AB_777047) was performed using the multiplex immunofluorescence technology of the Ventana Discovery Ultra automated stainer (RRID:SCR_021254) with PerkinElmer opal seven-color dyes. The whole slides were stained. In short, 3-µm FFPE sections were cut and heated at 75°C for 28 minutes and subsequently deparaffinized in EZ prep solution (Ventana Medical Systems). Using cell conditioning 1 (Ventana Medical Systems), heat-induced antigen retrieval was conducted at 95°C for 32 minutes. Further analysis was conducted via VECTRA image acquisition (Akoya

Biosciences, v3.0) and HALO (RRID:SCR_018350, Indica Labs, v2.3) image analysis. In the first data acquisition step, all tumor areas that were properly stained were included by manual selection. Next, tumor and stroma regions were classified by HALO automated tissue segmentation primarily based on PanCK expression. Adjacent stroma was defined as all tissue surrounding the tumor area within 150 µm. The area selected by HALO based on this parameter was then visually inspected for accuracy and subsequently used for cell segmentation, quantification, and analysis. Cell segmentation was performed using a pretrained nuclear segmentation AI module in HALO. Marker thresholds were manually set for each sample. Data were analyzed separately for tumor and stroma regions and subsequently exported. Immune cell classification was based on marker expression (Table 1).

When a cell was positive for two or more mutually exclusive markers, the cell was classified according to the highest relative intensity of the respective markers.

Computational analysis of multiplex immunofluorescence data

The final classification of cells into tumor and stromal regions and quantification of these regions' areas was performed by the method we previously published (12) with a modification to take into account immune cells in addition to the negative cells while computing stroma-related kernel density estimation. Initially, cell densities were obtained from the output of this step by dividing cell counts over the corresponding area. The density of the total cells (regardless of their label) was significantly higher in TUR-BT samples than in cystectomy (Supplementary Fig. S2A). To minimize possible bias related to this sample type, we switched to cell percentages by dividing each cell density by the total cell density.

We quantified spatial relationships using the first-nearest neighbor statistics for 49 (7×7) cell type pairs in our mIF data corresponding to the 7 cell types introduced in Table 1. After quantifying distances between the first-nearest neighboring cells of different cell types in the full analyzed area (tumor plus adjacent stroma), we fitted the Weibull distribution to these data using the generalized linear mixed effect models for each of the 49 cell type combinations in our mIF data following (12). The scale and shape parameters were used to calculate medians of the Weibull distribution. Before analyzing the medians, we performed the same analysis with the cell labels removed and compared the medians between the two sample types to control for possible bias. These overall medians were the same between the sample types (Supplementary Fig. S2B).

RNA-seq computational analysis

Gene expressions were quantified with Kallisto (v0.46.1, RRID:SCR_016582) with the Gencode (RRID:SCR_014966) reference transcriptome v40 (basic annotation). Gene transcripts per million values were filtered according to the gene biotype from the general transfer format (GTF) transcriptome annotation file, renormalized to 1 million in total, and used for ssGSEA (Gseapy v0.10.7). The following types of genes (according to the Gencode GTF basic annotation, v40) were retained in the expression files: "protein_coding," "processed_pseudogene," "transcribed_processed_pseudogene," "TEC," "polymorphic_pseudogene," "pseudogene," "IG_C_gene," "TR_C_gene," "translated_processed_pseudogene," and "IG_C_pseudogene." Transcript counts were summarized to the gene level and used for differential expression with DESeq2 (v1.36.0, RRID:SCR_015687) and gene set enrichment analysis (GSEA) with Fgsea (v1.22.0, RRID:SCR_020938) and Msigdb (v7.5.1, RRID:SCR_022870). The dataset

Table 1. Cell classification in the mIF data.

Marker positivity ^a	Cell type
PanCK ⁺	Cancer cell
CD8 ⁺ FoxP3 ⁻	CD8 ⁺ T cell
CD8 ⁻ FoxP3 ⁺	Treg
CD3 ⁺ CD8 ⁻ FoxP3 ⁻	T helper
CD68 ⁺	Macrophage
CD20 ⁺	B cell

^aAll cells were DAPI positive.

included two batches with differences in the library preparation protocol and sequencing. The batch correction procedure was performed with the Limma R package (v3.52.4, RRID:SCR_010943, function `removeBatchEffect`) on logarithmed gene transcripts per million expressions.

Statistical analysis

Pandas v1.3.3 (RRID:SCR_018214) and NumPy v1.20.0 (RRID:SCR_008633) were used for data handling. Seaborn v0.12.2 (RRID:SCR_018132), Matplotlib v3.7.3 (RRID:SCR_008624), Statannotations 0.4.2, and EnhancedVolcano v1.14.0 (RRID:SCR_018931) were used for plotting. Basic statistical tests were implemented from Scipy v1.8.1 (RRID:SCR_008058) and Statsmodels v0.13.1 (RRID:SCR_016074). Before comparison, Kendall τ -*b* correlation coefficients were transformed to the equivalent Pearson R using Kendall's formula (13). Function `r.test` from R package Psych (v2.3.9, RRID:SCR_021744) was used to perform a *z*-test of the difference of the Fisher's *z*-transformed correlations divided by the standard error of the difference.

For the analysis of the association between different chemotherapy regimens and changes in the TME, we used robust analogs of a mixed ANOVA: a rank-based, nonparametric method for longitudinal data in factorial experiments [F1-LD-F1 design (14), R package `nparLD`, v2.2] and the robust mixed ANOVA based on the trimmed means (R package `WRS2`, v1.1.5; ref. 15). For the variables violating the assumption of normality within each combination of the ANOVA model factors (macrophage cell percentage, CD8⁺ T-cell/macrophage-to-cancer-cell median 1-NN distances, and PDL1 IC), we applied the nonparametric method. Normality was tested using the Shapiro-Wilk test implemented in R package `Rstatix` (v0.7.2, RRID:SCR_021240).

Data availability

RNA-seq data have been deposited in the European Genome-phenome Archive under the accession code EGAS50000000309. Requests for RNA-seq and multiplex immunofluorescence data for academic use will be reviewed by the IRB of the Netherlands Cancer Institute; the researcher will need to sign a data access agreement with the Netherlands Cancer Institute after approval. Requests, up to six years of publication, can be directed to the corresponding author. Processed mIF and IHC data and RNA-seq-based signature scores generated in this study are available within the article and its Supplementary Data. Code to reproduce the main findings is available in a Github repository: https://github.com/mchelushkin/chemo_and_bladder_TME.

Results

Cohort and data description

We retrospectively included 183 patients with MIBC treated with platinum-based NAC followed by radical cystectomy (Supplementary

Fig. S1; "Materials and Methods"). Patients achieving a pCR to NAC have a favorable clinical outcome and are, therefore, less likely to benefit from additional ICI treatment; these patients were not included in the various adjuvant ICI studies for this reason (6). Furthermore, as all tumor cells will have been eliminated in patients with a pCR after neoadjuvant chemotherapy and prior to tissue collection, a reliable TME analysis cannot be conducted in these patients. Therefore, regardless of nodal status, only patients with remaining viable tumor tissue at cystectomy (\geq ypT1) were included (Supplementary Fig. S1).

Tissue samples from 130 patients were subjected to analysis. We collected pretreatment TUR-BT tissue at diagnosis (baseline) and posttreatment cystectomy tissue (resected tumor bulk) from each patient (Fig. 1A). In total, 116 unique patients represented by at least one sample of one data type (mIF, IHC, or RNA-seq) were included in our dataset; samples of 14 patients were of low quality (Supplementary Fig. S1). Sixty-two (53%) patients had clinically node-negative disease at baseline (cT2-4aN0), and 54 (47%) patients were clinically node-positive (cT2-4aN1-3, Table 2). Cisplatin was the most frequently used platinum-based treatment agent (78% of patients). Other patients were treated with carboplatin (12%) or switched their platinum agent during neoadjuvant treatment due to toxicity (8%). Of note, although cisplatin-based chemotherapy is the standard treatment in the neoadjuvant setting, some locoregionally advanced cis-ineligible patients were treated with carboplatin-based induction therapy and had consolidative surgery in case of clinical response. As the active metabolites between these platinum agents are similar (16) and questions regarding a potential difference in immune induction remain unanswered, we included both platinum agents. In addition to platinum, the treatment regimen included gemcitabine (in 66% of patients), MVAC (28%), or both at different time points (3%). The majority of patients (78%) received four cycles of NAC, whereas a subset received fewer (10%) or more (10%) than four cycles (Table 2).

The processed sample counts for each experimental technique and time point are shown in Fig. 1B and C. Due to failed quality control, not all patients had both TUR-BT and cystectomy samples processed successfully. The final number of paired samples included 85 pairs of mIF, 76 pairs of RNA-seq, and 79 pairs of PDL1 IHC. In 59 patients, all three analyses could be performed on paired samples (Fig. 1D).

Chemotherapy-induced changes in ICI response biomarkers

The abundance of tumor-infiltrating CD8⁺ T cells, PDL1 expression, and gene signatures related to T-cell immunity (e.g., IFN γ and effector CD8⁺ T-cell gene signatures) are biomarkers commonly associated with ICI response in cancer, including MIBC (17–19). We assessed CD8⁺ T-cell infiltration of tumors using mIF data. Because we used different sample types for our analyses—TUR-BT samples as prechemotherapy tissue and radical cystectomy samples after chemotherapy—we aimed to identify and mitigate possible biases in the mIF data analysis. After identifying a difference in the total cell density between the sample types (Supplementary Fig. S2A), we proceeded with cell percentages (normalized densities) instead of raw densities to minimize a possible confounding effect of the sample type ("Materials and Methods"). In our cohort, the CD8⁺ T-cell percentage (mIF) increased in the tumor area ($P = 0.015$, medians 1.3% and 2.0%) and adjacent stroma ($P = 0.017$, medians 5.1% and 6.5%; see "Materials and Methods") as well as in their combined area ($P = 0.00076$, medians 2.3% and 4.2%; Fig. 2A–C) upon chemotherapy treatment. The percentage of PDL1 positive

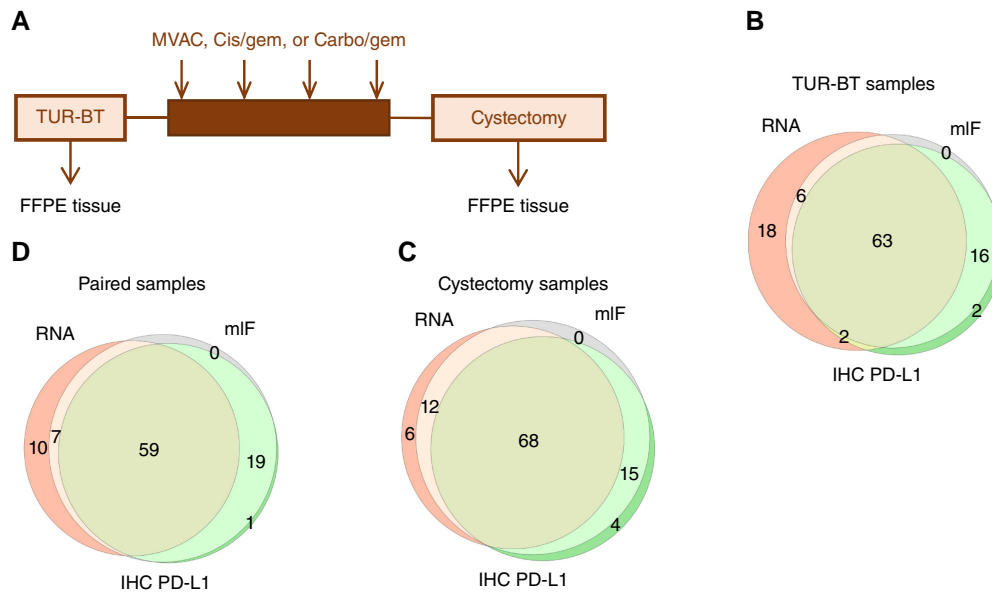


Figure 1. Treatment scheme (A) and collected data (B–D). B, Availability of pretreatment (TUR-BT) data by type. C, Availability of posttreatment (cystectomy) data by type. D, Number of sample pairs (TUR-BT-cystectomy from the same patient) available.

ICs, determined by IHC, increased after treatment ($P = 0.00033$, medians 6% and 11%; Fig. 2D), whereas the percentage of PDL1 positive TCs and the PDL1 CPS remained unchanged (Fig. 2E and F).

A fibroblast-based TGFβ signaling gene signature was previously associated with ICI resistance in MIBC in subsets of patients (17, 18, 21).

The single-sample GSEA (ssGSEA) score of this signature increased upon chemotherapy treatment in our cohort ($P = 2.1 \times 10^{-8}$; Fig. 2G). No difference in IFNγ and effector CD8+ T-cell gene signatures between pre- and postchemotherapy tumor tissue was detected (Fig. 2H and I). These results demonstrate that features both positively (CD8+ T-cell percentage and PDL1 IC score) and negatively (TGFβ signaling in fibroblasts) associated with ICI response in MIBC increased upon platinum-based chemotherapy.

Table 2. Patient and tumor characteristics and treatment information.

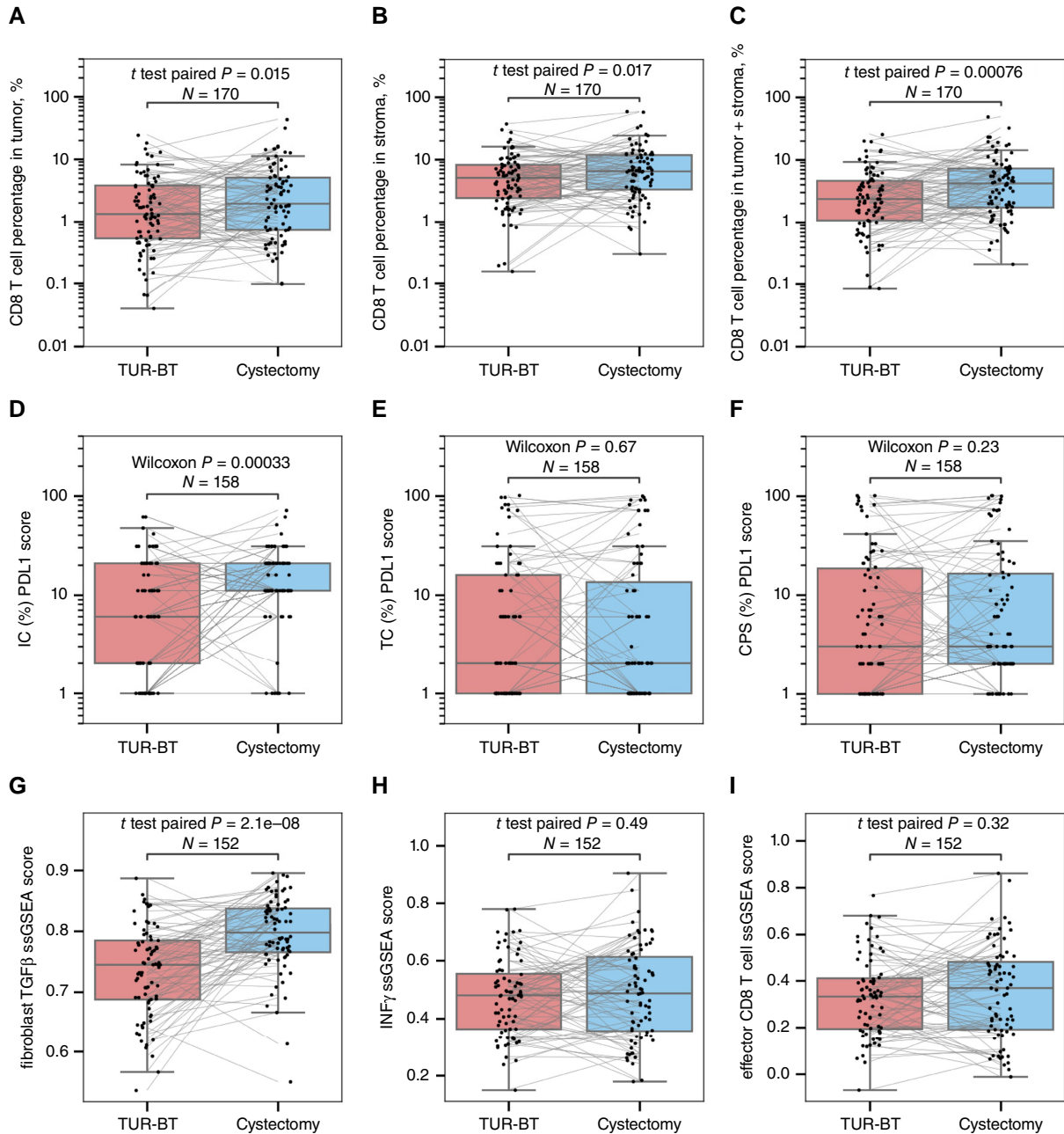
Patient and tumor characteristics	Total (n = 116)
Median age, years (range)	62 (31–86)
Male sex, n (%)	83 (72%)
Clinical classification at baseline	
cT2-4N0	62 (53%)
cT2-4N1-3	54 (47%)
Pathological classification at cystectomy	
ypT2-4N0-x	62 (53%)
ypT1-4N1-3	54 (47%)
Platinum chemotherapy agent	
Cisplatin	91 (78%)
Carboplatin	14 (12%)
Switched	9 (8%)
Unknown	2 (2%)
Chemotherapy regimen	
MVAC	33 (28%)
Gemcitabine + cisplatin or carboplatin	77 (66%)
Switched	4 (3%)
Unknown	2 (2%)
Total number of chemotherapy cycles	
4	90 (78%)
<4	12 (10%)
>4	12 (10%)
Unknown	2 (2%)

Comprehensive assessment of TME changes upon chemotherapy treatment

Next, we aimed to better understand the effect of platinum-based chemotherapy on the bladder cancer TME in a more comprehensive and unsupervised manner. We assessed alterations in the cellular immune cell composition by mIF and transcriptional changes through RNA-seq data by comparing pre- and postchemotherapy samples. Comparison of TME cell percentages assessed by mIF analysis showed that apart from the CD8+ T-cell percentage increase after chemotherapy, the macrophage cell percentage increased as well (adj. $P = 0.016$; Fig. 3A). Boxplots of cell percentages and raw densities of all cell types identified by our mIF panel between TUR-BT and cystectomy sample sets are shown in Supplementary Fig. S3.

GSEA performed with the hallmark gene sets (22) on the differentially expressed genes before and after treatment showed (among others) a strong upregulation of epithelial-mesenchymal transition (EMT; adj. $P = 5.5 \times 10^{-27}$) and TNFα-via-NF-κB signaling (adj. $P = 3.0 \times 10^{-33}$; Fig. 3B). Of note, EMT signaling was previously associated with ICI resistance in urothelial cancer (23).

We recently showed that a shorter distance from macrophages and CD8+ T cells to their first-nearest neighboring (1-NN) cancer cells at baseline was positively associated with preoperative combination ICI response in an analysis of the NABUCCO (MIBC) and IMCISION (head and neck cancer) trials (21, 24, 12). Following the same approach, we quantified the median 1-NN distances for each

**Figure 2.**

Changes associated with platinum-based chemotherapy. **A–C**, CD8⁺ T-cell percentage determined by mIF in the tumor (**A**), stromal areas (**B**), and full analyzed area (**C**). **D**, Percentage of PDL1-positive ICs determined by IHC. **E**, Percentage of PDL1-positive TCs determined by IHC. **F**, PDL1 CPS determined by IHC. **G**, ssGSEA score of the fibroblast-based TGF β signaling gene signature from ref. 17. **H** and **I**, ssGSEA score of interferon gamma and CD8⁺ T-cell effector gene signatures from refs. 19, 20. ssGSEA, single-sample gene set enrichment analysis. Numbers of samples are shown. Only paired samples are included in the analysis.

spatial relationship as identified by our mIF panel (refer to the “Materials and Methods” section for more details). To determine possible bias between the sample types, we analyzed the cell-type-agnostic 1-NN median distances. We established that they were similar between TUR-BTs and cystectomies (“Materials and Methods”; Supplementary Fig. S2B), suggesting no bias in the

analysis of 1-NN median distances. A comparison of paired cystectomies and TUR-BTs showed that all five immune cell types tested (CD8⁺ T cells, macrophages, Tregs, helper T cells, and B cells) were, on average, further away from their 1-NN cancer cells after chemotherapy treatment compared with the pretreatment sample (**Fig. 3C**), including CD8⁺ T cells ($P = 4.3 \times 10^{-7}$) and

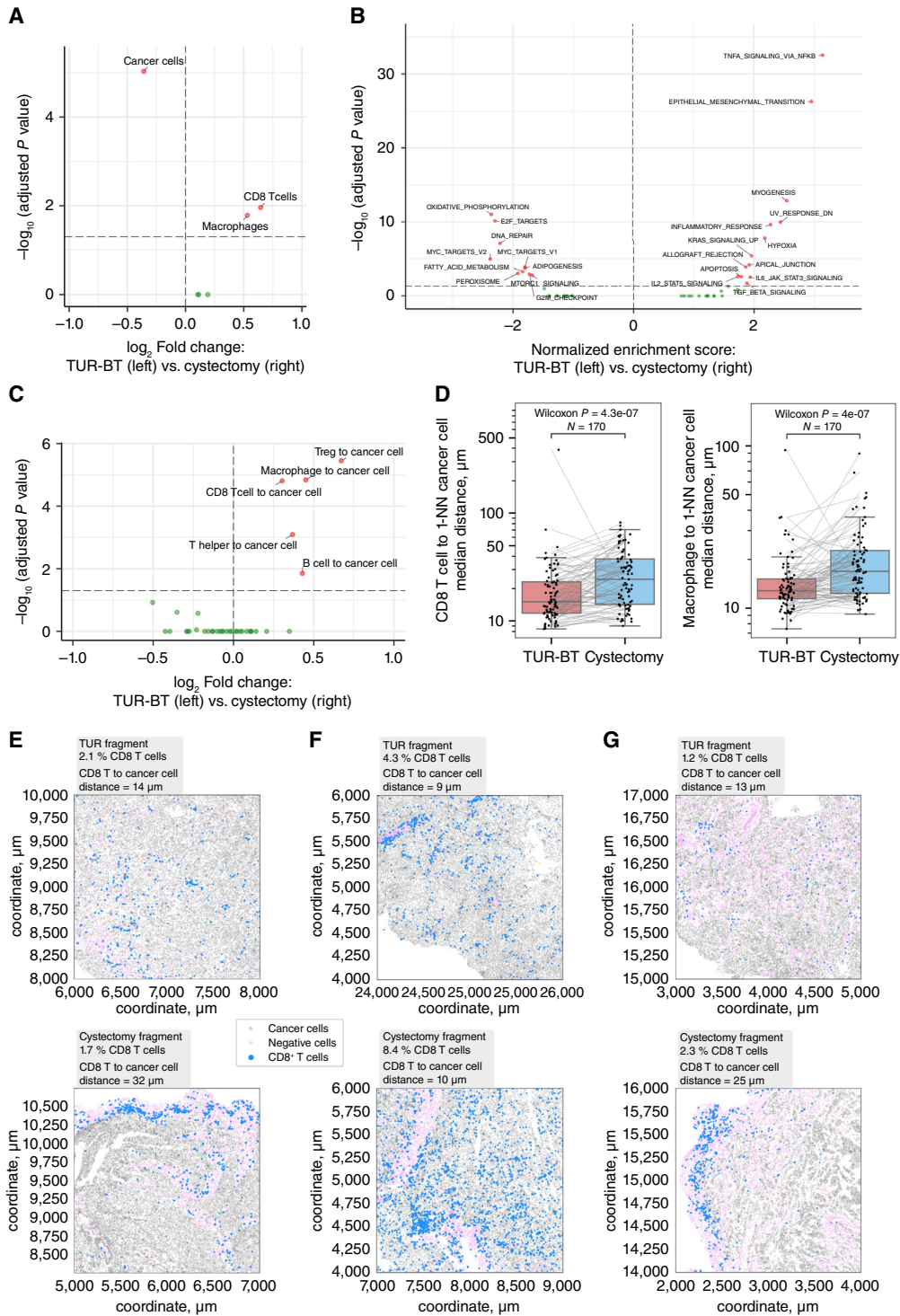


Figure 3.

A, mIF-based cell percentages compared between post- and pretreatment. **B**, GSEA results for hallmark gene signatures. **C**, 1-NN median distances calculated from fitting Weibull distribution to the mIF data and compared between post- and pretreatment. **D**, Comparison of median distances from CD8⁺ T cells to 1-NN cancer cells and from macrophages to 1-NN cancer cells between post- and pretreatment. Number of samples is shown. Only paired samples are included in the analysis. **E-G**, Examples of slide fragments for corresponding paired TUR-BT and cystectomy samples recreated based on cell coordinates and labels. Cell percentages and distances denoted correspond to the full analyzed area of the slides. Only CD8⁺ T cells (blue), cancer cells (gray), and DAPI-positive cells negative with the other markers (purple) are shown. P values shown in **A** and **C** are Wilcoxon test P values adjusted with Bonferroni correction for multiple testing. GSEA, gene set enrichment analysis.

macrophages ($P = 4.0 \times 10^{-7}$; **Fig. 3D**). Thus, although the percentages of cells with potential antitumor immune activity increased upon chemotherapy, immune cells were (on average) further from the nearest neighboring cancer cells. This increased distance suggests that their antitumor activity was possibly impeded. Fold changes in CD8⁺ T-cell percentages did not correlate with the fold changes in median distances from CD8⁺ T cells to 1-NN cancer cells (Supplementary Fig. S4). Therefore, in many sample pairs, only one of the two characteristics increased (Supplementary Fig. S4, examples in **Fig. 3E** and **F**). Still, in some sample pairs, both characteristics increased (Supplementary Fig. S4, examples in **Fig. 3G**).

Correlation analyses suggest different TME response patterns to chemotherapy

Next, we investigated whether changes in stromal (fibroblast TGF β and EMT) and inflammation-related (TNF α -via-NF- κ B) signatures correlated with specific changes in the TME immune cell composition upon treatment with chemotherapy. For this analysis, we considered immune cell percentages and distances that changed after chemotherapy treatment, i.e., CD8⁺ T-cell and macrophage percentages and all five immune-to-cancer cell distances (**Fig. 3A** and **C**), as well as the PDL1-positive immune cell percentage (**Fig. 2D**). For the correlation analysis, we used the Kendall τ - b correlation coefficient (because of ties in the PDL1 data). Results of the Pearson correlation analysis, excluding PDL1 IC data, are shown in Supplementary Fig. S5A–S5C. We found an association between the increase in CD8⁺ T-cell percentage and upregulation of TNF α -via-NF- κ B signaling upon chemotherapy (τ - $b = 0.31$, $P = 0.00022$; **Fig. 4A**; Supplementary Fig. S6A). The TNF α -via-NF- κ B signature and CD8⁺ T-cell percentage also correlated significantly after chemotherapy, i.e., within the cystectomy sample set (τ - $b = 0.23$, $P = 0.0024$; **Fig. 4B**; Supplementary Fig. S6B), and before chemotherapy, i.e., within the TUR-BT sample set (τ - $b = 0.23$, $P = 0.0050$; **Fig. 4C**; Supplementary Fig. S6C). These results suggest that a subset of patients experienced an induction of T-cell immunity upon platinum-based chemotherapy, e.g., patients with a higher than median change in TNF α -via-NF- κ B signaling showed a higher fold change in CD8⁺ T-cell infiltration ($P = 0.00028$; **Fig. 4D**).

In contrast, the fibroblast-based TGF β signaling positively correlated with higher distances (but not densities) from each immune cell type to their nearest cancer cell within posttreatment samples (**Fig. 4B** and **F**). Additionally, a negative correlation was observed between these distances and the PDL1 IC score (**Fig. 4B**). Furthermore, we investigated the correlation between PDL1 IC and fibroblast TGF β signaling. We found a significantly negative correlation (Supplementary Fig. S6D, τ - $b = -0.28$, $P = 0.0020$). When comparing high and low PDL1 IC in posttreatment samples based on the median PDL1 IC score (11%), the IC-low subset showed a higher fibroblast-derived TGF β signaling score [**Fig. 4E** (right)] and larger distances from immune cells to their nearest cancer cells [regardless of their density; **Fig. 4G** (right)]. This was not observed when comparing TUR-BT samples split by the baseline PDL1 IC median [6%; **Fig. 4E** and **G** (left)]. Our previous work with NABUCCO samples found a negative correlation between pathologic response to preoperative immunotherapy and both fibroblast TGF β signaling (21) and 1-NN CD8-cancer cell distances (12). Therefore, we expect the TME in patients belonging to the subset with high postchemotherapy TGF β signaling and 1-NN CD8-cancer cell distance and low PDL1 IC score to be less likely to support response to ICI.

The associations found between TGF β , PDL1 IC positivity, and immune-to-cancer cell distances in the posttreatment set seemed to be weaker or absent before treatment (**Fig. 4C**). We formally tested which correlations changed upon treatment [using Fisher's z -transformation of the equivalent Pearson correlations ("Materials and Methods")] and found a statistically significant difference (FDR < 5%) for the immune cell distances to 1-NN cancer cells and PDL1 IC positivity (Supplementary Fig. S7, an example for CD8 T cells and IC is shown on Supplementary Fig. S6E and S6F). Although the correlation coefficient between the macrophage-to-cancer-cell distance and PDL1 IC score changed significantly (with FDR level < 5%), it was the pair with the weakest resulting correlation in the cystectomy set (**Fig. 4B**). These results suggest that the percentage of PDL1 positive cells among immune cells is higher when they are closer to their nearest neighboring cancer cells, and this relation appears only after chemo-treatment. For CD8⁺-T-cell-to-cancer-cell distances, this is illustrated in **Fig. 4G** with the PDL1 IC score binarized by medians.

MVAC and gemcitabine-containing platinum-based regimens were associated with distinct changes to the TME

Although all patients received platinum-based chemotherapy, the specific chemotherapeutic regimens varied (**Table 2**). To assess the impact of these regimens on TME changes, we explored differences between MVAC and gemcitabine-containing platinum-based regimens. We used robust analogs of mixed ANOVA with between-subject variable "chemo regimen" and within-subject variable "time-point," i.e., TUR-BT (pretreatment) or cystectomy (posttreatment; "Materials and Methods," Statistical analysis). We performed this analysis with each of the target variables, which are the TME characteristics changed upon chemotherapy [CD8⁺ T-cell and macrophage cell percentages (**Fig. 3A**), PDL1 IC, fibroblast TGF β (**Fig. 2D** and **G**), CD8⁺-T-cell-to-cancer median 1-NN distance, and macrophage-to-cancer median 1-NN distance (**Fig. 3C** and **D**)]. In addition to significant coefficients for the timepoint term in all models (in line with the overall changes shown in **Figs. 2** and **3**), our analyses showed significant statistical interaction between the timepoint and chemo regimen variables in the models for the macrophage cell percentage and fibroblast TGF β signaling (**Fig. 5A**). These results suggest that the change in macrophage cell percentage and fibroblast TGF β signaling depended on the regimen, whereas the changes in CD8⁺ T-cell density, PDL1 IC, CD8⁺-T-cell-to-cancer cell, and macrophage-to-cancer cell median 1-NN distances were the same for both regimens. The post-hoc analysis showed a more pronounced increase in the macrophage cell percentage upon MVAC than upon gemcitabine-containing chemotherapy (**Fig. 5B**). Conversely, fibroblast TGF β signaling increased more upon the gemcitabine-containing platinum-based regimen (**Fig. 5C**). We did not find associations with the type of platinum agent (cisplatin vs. carboplatin) for the six TME characteristics analyzed before in the context of MVAC and gemcitabine-containing platinum-based regimens (Supplementary Fig. S8). However, the analysis of the platinum agent had less statistical power and a more unbalanced design due to the small number of carboplatin-treated patients (eight patients with paired mIF and 11 patients with paired RNA data) compared with the number of cisplatin-treated patients (68 patients with paired mIF and 57 patients with paired RNA data). Given the clinical importance of potentially stronger immune modulation by cisplatin than carboplatin, we reanalyzed the subcohort of patients treated with cisplatin-based chemotherapy using the same methods as in the entire cohort (Supplementary Figs. S9–S12). The overall conclusions from the reanalyses were similar to the

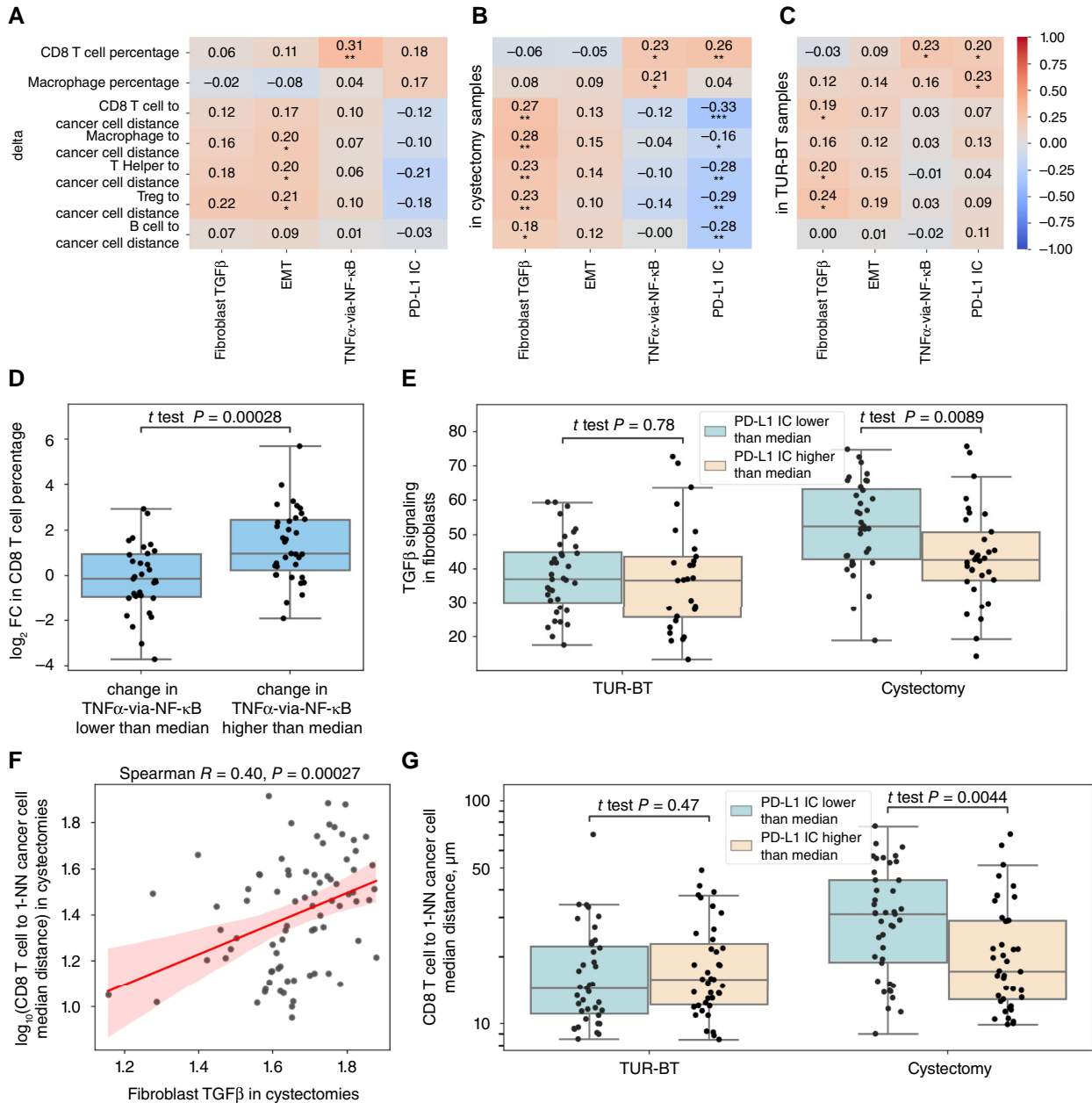


Figure 4. A-C, Correlation analysis of parameters altered by the chemo-treatment between different data modalities. RNA-seq and IHC are shown on the x-axis, and mIF is shown on the y-axis. Kendall τ -b correlation coefficients are shown and indicated by colors. Stars denote P values for the correlation coefficients to be nonzero assessed by the distribution of τ (two-sided test): *, $P < 0.05$; **, $P < 0.01$; ***, $P < 0.001$. P values are FDR-adjusted for multiple testing within each column. **A**, Correlations between changes (“deltas”). **B**, Correlations within cystectomy samples (posttreatment). **C**, Correlations within TUR-BT samples (pretreatment). **D**, Comparison of CD8⁺ T-cell percentage (mIF) fold change upon chemo-treatment between patient groups with the change in TNFα-via-NF-κB gene signature score (RNA) below and higher than a median change. **E**, Comparison of fibroblast-derived TGFβ gene signature score (RNA) between groups of TUR-BT and cystectomy samples with the PDL1 IC score lower and higher than the TUR-BT median and the cystectomy median correspondingly. **F**, Correlation between the fibroblast-derived TGFβ gene signature score (RNA) and CD8⁺-T-cell-to-cancer-cell 1-NN median distance (mIF) in cystectomy samples. **G**, Comparison of CD8⁺-T-cell-to-cancer-cell 1-NN median distance between groups of TUR-BT and cystectomy samples with the PDL1 IC score lower and higher than the TUR-BT median and the cystectomy median correspondingly.

full cohort, and minor differences might be explained by a limited loss of statistical power due to the decreased sample size.

Finally, we applied the robust analogs of mixed ANOVA to assess whether the TME changes differed between patients who continued to

have muscle-invasive disease after chemotherapy and those who had ypT1 non-muscle-invasive disease at pathology. The latter group consisted of only six patients (five in each of the analyses) with available paired data. This analysis showed significant statistical

Target variable	CD8 ⁺ T cell fraction (mIF)	Macrophage cell fraction (mIF)	PD-L1 IC	Fibroblast-derived TGF β signaling (ssGSEA score)	CD8 ⁺ T cell to cancer cell median 1-NN distance	Macrophage to cancer cell median 1-NN distance
Method	mixed ANOVA based on the trimmed means	F1-LD-F1 non-parametric model, ANOVA	F1-LD-F1 non-parametric model, ANOVA	mixed ANOVA based on the trimmed means	F1-LD-F1 non-parametric model, ANOVA	F1-LD-F1 non-parametric model, ANOVA
Chemo regimen, <i>P</i> value	0.85	0.074	0.013	0.15	0.83	0.35
Time point, <i>P</i> value	0.0056	0.00012	1.0×10^{-5}	9.0×10^{-7}	3.2×10^{-7}	1.4×10^{-6}
Chemo regimen: Time point, interaction <i>P</i> value	0.66	0.023	0.13	0.026	0.84	0.66

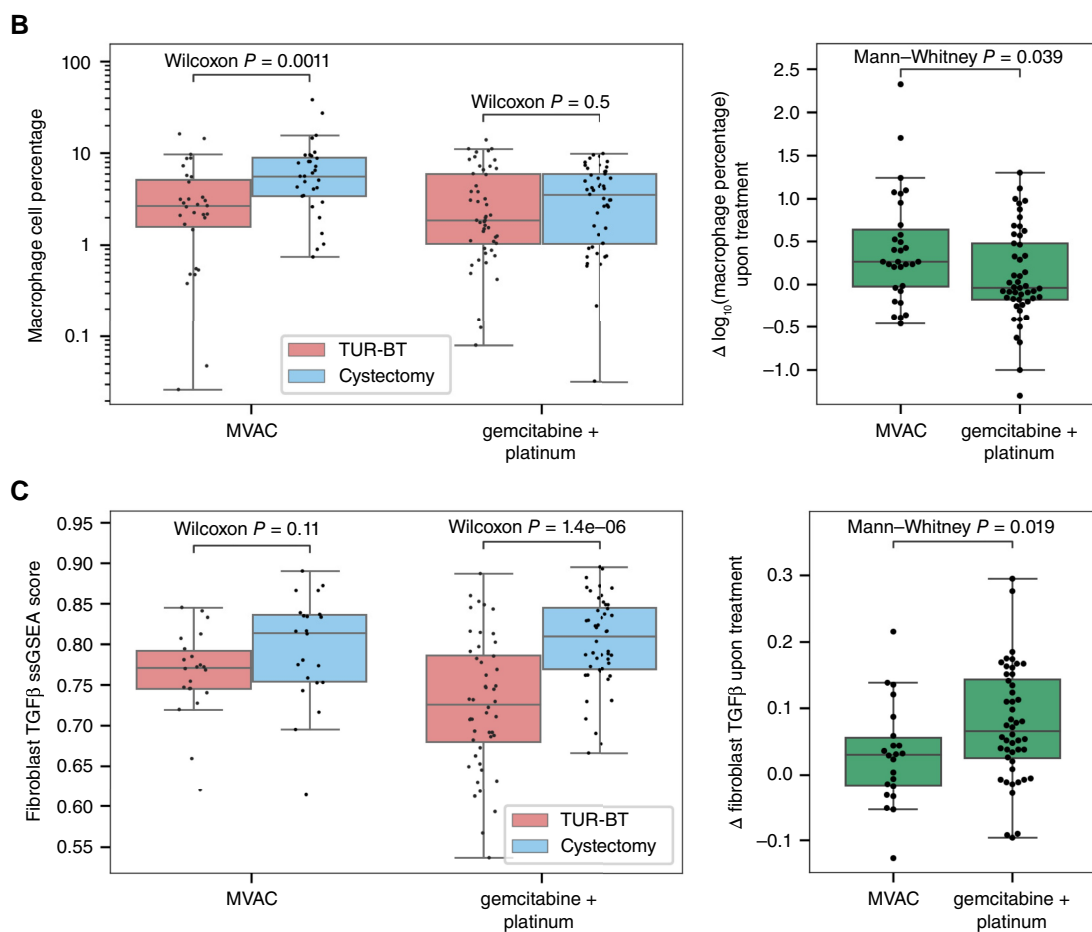


Figure 5.

Analysis of changes in the TME characteristics upon MVAC and gemcitabine-containing platinum-based chemotherapy regimens. **A**, *P* values of robust mixed ANOVA analogs [chosen depending on the data normality for each combination of the ANOVA design factors (“Materials and Methods,” Statistical analysis)]. Significant statistical interactions between the regimen and time point are highlighted as bold. **B** and **C**, *Post hoc* analysis of changes in macrophage cell percentage (**B**) and fibroblast-derived TGF β signaling (**C**). The left panels compare pre- and posttreatment groups of patients who received different chemotherapy regimens. The right panels show comparison between changes (“deltas”) upon the distinct regimens.

interaction between the timepoint and response variables in the models for the median distances from CD8⁺ T cells and macrophages to the 1-NN cancer cells (Supplementary Fig. S13A). The post-hoc analysis (Supplementary Fig. S13B and S13C) showed that both median distances increased significantly more in nonresponders ($P = 0.009$ and 0.003), suggesting a partial response to NAC as a positive event regarding chemo-induced immune modulation.

In summary, our results show that platinum-based chemotherapy can induce changes that are potentially either pro-immunogenic (increased CD8⁺ T-cell percentage, TNF α -via-NF- κ B signaling, and IC PDL1 score) or immune-inhibitory (larger distance of immune-to-cancer cells and stromal signatures).

Discussion

The efficacy of concurrent chemotherapy and ICI has been established in lung, head and neck, triple-negative breast, gastric, and esophageal cancers (25). In urothelial cancer, clinical trials yielded inconsistent results (6, 7, 8, 10, 11, 26). In this study, we comprehensively assessed the TME in urothelial bladder cancer following platinum-based chemotherapy. To do so, we have collected and analyzed a large dataset of paired pre- and post-platinum-treatment bladder tumor samples analyzed with different experimental techniques.

In our cohort of patients with MIBC treated with platinum-based chemotherapy, several parameters indicative of T-cell immunity increased. This included an increase in the CD8⁺ T-cell percentage, determined by mIF, and in the percentage of PDL1⁺ immune cells, determined by IHC; upregulation of TNF α -via-NF- κ B, as shown in differential gene expression analysis, was also noted. The macrophage (CD68⁺) percentage increased as well, which was specifically associated with the MVAC treatment regimen.

Several preclinical studies have suggested an association between cisplatin chemotherapy and increased CD8⁺ T-cell infiltration or activation (27–29). Single-cell RNA-seq analysis of peripheral blood immune cells of patients with metastatic urothelial cancer in the IMvigor130 trial at baseline and on chemotherapy demonstrated that cisplatin (and not carboplatin; both with gemcitabine) induced immune and inflammatory transcriptional programs in circulating monocytes, including TNF α -via-NF- κ B, and genes encoding proteins associated with antigen presentation and T-cell priming (30). Seiler and colleagues (31) found specific postchemotherapy molecular subtypes in MIBC, some of which were characterized by higher immune signatures and CD8⁺ T-cell immune infiltration. In contrast, a recent study in human bladder cancer showed no association between neoadjuvant platinum-based chemotherapy and CD8⁺ T-cell infiltration assessed by mIF (32). However, the sample size in the latter study (33 patients) was smaller than that in our cohort, and a comparison was made with raw cell densities (cells per mm²) rather than percentages, potentially amplifying confounding signals from the different sample types (“Materials and Methods”). Evidence for platinum chemotherapy-induced immune modulation has been found in multiple studies on other cancer types (33–36).

In contrast to these alterations related to an enhanced immune presence in the tumor, potentially indicative of a favorable ICI response, several parameters previously connected with ICI resistance increased upon chemotherapy. Expression of a fibroblast-derived TGF β gene signature was enhanced after chemotherapy. Its upregulation was significantly higher in the tumors of patients treated with a gemcitabine-containing platinum-based regimen (in contrast to MVAC). In line with our results, a recent report suggests that platinum chemotherapy drug accumulation in cancer-

associated fibroblasts intensified TGF β activity and was associated with increased cancer aggressiveness in colorectal cancer (37). Additionally, median distances from CD8⁺ T cells and macrophages to their nearest neighboring cancer cell increased upon chemotherapy and were significantly correlated with the fibroblast-based TGF β signaling in posttreatment samples. Interestingly, spatial analysis of triple-negative breast cancer in mice showed that quiescent cancer cells expressing chemotherapy resistance genes form niches that exclude immune infiltrates locally and contain immune-suppressive fibroblasts (38). In our approach, local exclusion corresponds to the increase in 1-NN distances from immune cells to cancer cells.

Our findings may point to the importance of a balance between pro-immunogenic and anti-immunogenic aspects of the bladder cancer TME, ultimately determining the response to ICI treatment. The importance of such opposing forces in the TME was previously suggested by Wang and colleagues (23), showing that in patients with T-cell infiltrated tumors, higher EMT/stroma-related gene expression is associated with lower clinical benefit to nivolumab in advanced urothelial cancer. Similarly, Mariathasan and colleagues (17) showed that a gene signature related to TGF β signaling in fibroblasts was inversely associated with response to atezolizumab, specifically in immune-excluded tumors. Our findings suggest that platinum-based chemotherapy can modulate this balance in a positive or negative way.

The chemotherapy-associated TME alterations discussed above indicate several potential avenues to improve the benefit of chemotherapy and immunotherapy combinations. The addition of TGF β inhibitors to ICI regimens after platinum-based NAC, especially in regimens containing gemcitabine, may improve immunotherapeutic responses in MIBC. Combinations of ICI and TGF β inhibitors have been tested in phase I and II clinical trials in various cancer types, including urothelial cancer (39). However, although preclinical studies exploring the combination of TGF β and PD1/PDL1 inhibition showed uniformly positive results, the addition of TGF β inhibitors in clinical trials has often failed to show a meaningful benefit beyond the current generation of ICIs alone (39). Administering agents promoting spatial rearrangement of immune cells to achieve closer proximity to cancer cells, e.g., bispecific antibodies, might be another treatment option, specifically in the setting of ICI after platinum-based NAC. Several bispecific antibodies targeting cancer cells and T cells have been tested in clinical urothelial cancer trials (40, 41). Interestingly, therapeutic coadministration of TGF β inhibitors and PDL1 inhibitors in a mouse mammary carcinoma model recapitulating an immune-excluded phenotype was shown to facilitate T-cell penetration into the center of tumors and provoke tumor regression, whereas therapeutic blockade of PDL1 or TGF β alone had little or no effect (17).

This study has several limitations. First, we used different sample types for our analyses: TUR-BT samples as prechemotherapy tissue and radical cystectomy samples after chemotherapy. Indeed, total cell densities were different between TUR-BT and cystectomy, which may have been caused by tissue acquisition and preparation or by chemotherapy-related changes in tumor composition. The influence of extratumoral stroma (which would be more abundant in cystectomy samples) was minimized by selecting only a limited area (<150 μ m from tumor cells) for our mIF analysis. We further aimed to mitigate possible biases in the mIF analysis using cell percentages of total cells instead of raw densities. Additionally, the TUR-BT procedure itself may induce inflammation, which could have biased our results. A study by van Wilpe and colleagues (32) showed no CD8⁺

T-cell infiltration increase due to TUR-BT. A set of TUR-cystectomy pairs that did not receive NAC showed an increase in PDL1 on immune cells (but not tumor cells; Supplementary Fig. S14). However, the time between TUR-BT and cystectomy was short (around 2 months), whereas it was 5 to 6 months in our NAC-treated cohort due to the administration of several cycles of neoadjuvant chemotherapy. Due to the much shorter time between the TUR-BT procedure and cystectomy, the untreated population is likely to be more susceptible to procedure-induced inflammation than the chemo-treated population. Another limitation is the heterogeneity in the chemotherapy regimens (Table 2). Although the inclusion of different regimens could have allowed us to study divergent effects on the TME by comparing cisplatin and carboplatin, only 12% of patients were treated with carboplatin, whereas 78% received cisplatin. This difference complicated the detection of TME-related changes associated with the specific platinum agent, which are of interest given the recent clinical results of CheckMate-901 study and the translational findings in peripheral immune cells of cisplatin- versus carboplatin-based chemotherapy in the IMvigor130 study (30, 10). Moreover, we report and discuss correlations between stromal (fibroblast TGF β and EMT) and inflammation-related (TNF α -via-NF- κ B) signatures with the TME immune cell composition that are relatively weak (Fig. 4). Furthermore, although our ultimate interest was motivated by establishing potential synergy or antagonism between chemo- and immunotherapies, patients in our cohort did not receive immunotherapy perioperatively. A dataset consisting of a pre- and post-NAC comprehensive TME assessment and clinical data on additional perioperative immunotherapy treatment does not exist currently. However, clinical studies randomizing between NAC with or without checkpoint inhibition are currently ongoing, and tumor tissue collected in these trials may provide a source for further validation (42). Our study does not provide information about whether TME modulation by chemotherapy is stable in time and affects the immune response to ICI at the time of its administration. Finally, extrapolating our findings to treatment in the adjuvant setting may be challenging as the analysis was conducted on the primary site (bladder) that was surgically removed. It remains unknown if the changes in the bladder TME translate into changes in the TME of the micrometastases, which would be ultimately treated with adjuvant ICI.

In conclusion, neoadjuvant platinum-based chemotherapy for MIBC is associated with promoting TME characteristics previously shown to relate to both ICI response (CD8⁺ T-cell percentage, PDL1⁺ immune cell percentage) and ICI resistance (fibroblast-based TGF β signaling, median distances from CD8⁺ T cells and macrophages to their nearest cancer cells). Additionally, our data suggest biological differences between MVAC and gemcitabine-containing platinum-based chemo regimens in terms of their effects on the bladder TME. A better understanding of chemotherapy-induced changes in the bladder TME and their implications for immunotherapy warrants further investigation. Future studies could test our hypotheses by analyzing data from patients randomized between NAC with and without concurrent ICI, with several ongoing phase III studies expected to provide relevant insights.

References

1. Witjes JA, Bruins HM, Cathomas R, Compérat EM, Cowan NC, Gakis G, et al. European association of urology guidelines on muscle-invasive and metastatic bladder cancer: summary of the 2020 guidelines. *Eur Urol* 2021;79:82–104.

Authors' Disclosures

M.A. Chelushkin reports grants from Bristol Myers Squibb (BMS) during the conduct of the study; in addition, M.A. Chelushkin has a patent for US11587642B2 issued to BostonGene Corporation, a patent for US20220119881A1 pending, a patent for US20220372580A1 pending, a patent for US20220375543A1 pending, and a patent for US20210005284A1 pending, and holds stock in BostonGene Corporation. J.-J.J. Mellema reports grants and nonfinancial support from Bristol Myers Squibb (BMS) during the conduct of the study. B.W.G. van Rhijn reports grants from BMS during the conduct of the study as well as other support from QED Therapeutics and Incyte International Biosciences outside the submitted work. L.S. Mertens reports other support from J&J and Merck outside the submitted work. N. Mehra reports grants and personal fees from AstraZeneca, Astellas, Sanofi, JNJ, and MSD and personal fees from Bayer outside the submitted work. L.F.A. Wessels reports grants from Bristol Myers Squibb outside the submitted work. M.S. van der Heijden reports grants and personal fees from BMS during the conduct of the study, as well as grants and personal fees from BMS, MSD, and AstraZeneca; grants from Roche and 4SC, and personal fees from Pfizer, Janssen, and Astellas outside the submitted work. No potential conflicts of interest were disclosed by the other authors.

Authors' Contributions

M.A. Chelushkin: Conceptualization, data curation, software, formal analysis, investigation, visualization, methodology, writing—original draft. **J. van Dorp:** Conceptualization, resources, data curation, investigation, methodology, project administration, writing—review and editing. **S. van Wilpe:** Resources, data curation, investigation, writing—review and editing. **I.M. Seignette:** Data curation, formal analysis, investigation, methodology, writing—review and editing. **J.-J.J. Mellema:** Data curation, investigation, writing—review and editing. **M. Alkemade:** Investigation, writing—review, and editing. **A. Gil-Jimenez:** Software, methodology, writing—review and editing. **D. Peters:** Resources, methodology, writing—review and editing. **W. Brugman:** Resources, investigation, writing—review and editing. **C.F. Stockem:** Investigation, writing—review, and editing. **E. Hooijberg:** Resources, methodology, writing—review, and editing. **A. Broeks:** Resources, methodology, writing—review and editing. **B.W.G. van Rhijn:** Resources, methodology, writing—review and editing. **L.S. Mertens:** Resources, methodology, writing—review and editing. **A.G. van der Heijden:** Resources, methodology, writing—review, and editing. **N. Mehra:** Resources, methodology, writing—review and editing. **M.L. van Montfoort:** Resources, investigation, writing—review and editing. **L.F.A. Wessels:** Conceptualization, resources, supervision, methodology, writing—review and editing. **D.J. Vis:** Conceptualization, resources, supervision, methodology, writing—review and editing. **M.S. van der Heijden:** Conceptualization, resources, supervision, funding acquisition, investigation, methodology, project administration, writing—review and editing.

Acknowledgments

We would like to thank all core facilities of the NKI for their help in this project and Charlotte Voskuilen and Elies Fransen van de Putte for their help in the collection of tumor samples. We would like to thank Audit DeBroy from BMS for support in the project. The Research High Performance Computing (RHPC) facility is acknowledged for providing computational facilities to perform the analysis. This study was funded by a BMS II-ON grant (OT123-416).

Note

Supplementary data for this article are available at Clinical Cancer Research Online (<http://clincancerres.aacrjournals.org/>).

Received March 6, 2024; revised May 8, 2024; accepted July 23, 2024; published first July 24, 2024.

2. Powles T, Bellmunt J, Comperat E, De Santis M, Huddart R, Loriot Y, et al; ESMO Guidelines Committee. Bladder cancer: ESMO Clinical Practice Guideline for diagnosis, treatment and follow-up. *Ann Oncol* 2022;33:244–58.

3. Yin M, Joshi M, Meijer RP, Glantz M, Holder S, Harvey HA, et al. Neoadjuvant chemotherapy for muscle-invasive bladder cancer: a systematic review and two-step meta-analysis. *Oncologist* 2016;21:708–15.
4. Pfister C, Gravis G, Fléchon A, Soulié M, Guy L, Laguerre B, et al. Randomized phase III trial of dose-dense methotrexate, vinblastine, doxorubicin, and cisplatin, or gemcitabine and cisplatin as perioperative chemotherapy for patients with muscle-invasive bladder cancer. Analysis of the GETUG/AFU V05 VESPER trial secondary endpoints: chemotherapy toxicity and pathological responses. *Eur Urol* 2021;79:214–21.
5. Advanced Bladder Cancer (ABC) Meta-analysis Collaboration. Neoadjuvant chemotherapy in invasive bladder cancer: update of a systematic review and meta-analysis of individual patient data advanced bladder cancer (ABC) meta-analysis collaboration. *Eur Urol* 2005;48:202–5.
6. Bajorin DF, Witjes JA, Gschwend JE, Schenker M, Valderrama BP, Tomita Y, et al. Adjuvant nivolumab versus placebo in muscle-invasive urothelial carcinoma. *N Engl J Med* 2021;384:2102–14.
7. Powles T, Park SH, Voog E, Caserta C, Valderrama BP, Gurney H, et al. Avelumab maintenance therapy for advanced or metastatic urothelial carcinoma. *N Engl J Med* 2020;383:1218–30.
8. Galsky MD, Arija JÁA, Bamias A, Davis ID, De Santis M, Kikuchi E, et al; IMvigor130 Study Group. Atezolizumab with or without chemotherapy in metastatic urothelial cancer (IMvigor130): a multicentre, randomised, placebo-controlled phase 3 trial. *Lancet* 2020;395:1547–57.
9. Grande E, Arranz JÁ, De Santis M, Bamias A, Kikuchi E, Del Muro XG, et al. Atezolizumab plus chemotherapy versus placebo plus chemotherapy in untreated locally advanced or metastatic urothelial carcinoma (IMvigor130): final overall survival analysis results from a randomised, controlled, phase 3 study. *Lancet Oncol* 2024;25:29–45.
10. van der Heijden MS, Sonpavde G, Powles T, Necchi A, Burotto M, Schenker M, et al. Nivolumab plus gemcitabine-cisplatin in advanced urothelial carcinoma. *N Engl J Med* 2023;389:1778–89.
11. Powles T, Csösz T, Özgüroğlu M, Matsubara N, Géczi L, Cheng SY-S, et al. Pembrolizumab alone or combined with chemotherapy versus chemotherapy as first-line therapy for advanced urothelial carcinoma (KEY-NOTE-361): a randomised, open-label, phase 3 trial. *Lancet Oncol* 2021;22:931–45.
12. Gil-Jimenez A, van Dijk N, Vos JL, Lubeck Y, van Montfoort ML, Peters D, et al. Spatial relationships in the urothelial and head and neck tumor micro-environment predict response to combination immune checkpoint inhibitors. *Nat Commun* 2024;15:2538.
13. Kendall MG. Rank correlation methods. 4th ed. London: Charles Griffin & Co; 1970. p. 126.
14. Noguchi K, Gel YR, Brunner E, Konietzschke F. nparLD: an R software package for the nonparametric analysis of longitudinal data in factorial experiments. *J Stat Softw* 2012;50:1–23.
15. Mair P, Wilcox R. Robust statistical methods in R using the WRS2 package. *Behav Res Methods* 2020;52:464–88.
16. Go RS, Adjei AA. Review of the comparative pharmacology and clinical activity of cisplatin and carboplatin. *J Clin Oncol* 1999;17:409–22.
17. Mariathasan S, Turley SJ, Nickles D, Castiglioni A, Yuen K, Wang Y, et al. TGF β attenuates tumour response to PD-L1 blockade by contributing to exclusion of T cells. *Nature* 2018;554:544–8.
18. Powles T, Kockx M, Rodriguez-Vida A, Duran I, Crabb SJ, Van Der Heijden MS, et al. Clinical efficacy and biomarker analysis of neoadjuvant atezolizumab in operable urothelial carcinoma in the ABACUS trial. *Nat Med* 2019;25:1706–14.
19. Ayers M, Lunceford J, Nebozhyn M, Murphy E, Loboda A, Kaufman DR, et al. IFN- γ -related mRNA profile predicts clinical response to PD-1 blockade. *J Clin Invest* 2017;127:2930–40.
20. Rosenberg JE, Hoffman-Censits J, Powles T, van der Heijden MS, Balar AV, Necchi A, et al. Atezolizumab in patients with locally advanced and metastatic urothelial carcinoma who have progressed following treatment with platinum-based chemotherapy: a single-arm, multicentre, phase 2 trial. *Lancet* 2016;387:1909–20.
21. van Dijk N, Gil-Jimenez A, Silina K, Hendricksen K, Smit LA, de Feijter JM, et al. Preoperative ipilimumab plus nivolumab in locoregionally advanced urothelial cancer: the NABUCCO trial. *Nat Med* 2020;26:1839–44.
22. Liberzon A, Birger C, Thorvaldsdóttir H, Ghandi M, Mesirov JP, Tamayo P. The Molecular Signatures Database (MSigDB) hallmark gene set collection. *Cell Syst* 2015;1:417–25.
23. Wang L, Saci A, Szabo PM, Chasalow SD, Castillo-Martin M, Domingo-Domenech J, et al. EMT- and stroma-related gene expression and resistance to PD-1 blockade in urothelial cancer. *Nat Commun* 2018;9:3503.
24. Vos JL, Elbers JBW, Krijgsman O, Traets JJH, Qiao X, van der Leun AM, et al. Neoadjuvant immunotherapy with nivolumab and ipilimumab induces major pathological responses in patients with head and neck squamous cell carcinoma. *Nat Commun* 2021;12:7348.
25. Larroquette M, Domblides C, Lefort F, Lasserre M, Quivy A, Sionneau B, et al. Combining immune checkpoint inhibitors with chemotherapy in advanced solid tumours: a review. *Eur J Cancer* 2021;158:47–62.
26. Bellmunt J, Hussain M, Gschwend JE, Albers P, Oudard S, Castellano D, et al. Adjuvant atezolizumab versus observation in muscle-invasive urothelial carcinoma (IMvigor010): a multicentre, open-label, randomised, phase 3 trial. *Lancet Oncol* 2021;22:525–37.
27. Wakita D, Iwai T, Harada S, Suzuki M, Yamamoto K, Sugimoto M. Cisplatin augments antitumor T-cell responses leading to a potent therapeutic effect in combination with PD-L1 blockade. *Anticancer Res* 2019;39:1749–60.
28. Markasz L, Skribek H, Uhlin M, Otvos R, Flaberg E, Eksborg S, et al. Effect of frequently used chemotherapeutic drugs on cytotoxic activity of human cytotoxic T-lymphocytes. *J Immunother* 2008;31:283–93.
29. Beyranvand Nejad E, van der Sluis TC, van Duikerken S, Yagita H, Janssen GM, van Veelen PA, et al. Tumor eradication by cisplatin is sustained by CD80/86-mediated costimulation of CD8⁺ T cells. *Cancer Res* 2016;76:6017–29.
30. Galsky MD, Guan X, Rishipathak D, Rapaport AS, Shehata HM, Bancheureau R, et al. Immunomodulatory effects and improved outcomes with cisplatin-versus carboplatin-based chemotherapy plus atezolizumab in urothelial cancer. *Cell Rep Med* 2024;5:101393.
31. Seiler R, Gibb EA, Wang NQ, Oo HZ, Lam H-M, van Kessel KE, et al. Divergent biological response to neoadjuvant chemotherapy in muscle-invasive bladder cancer. *Clin Cancer Res* 2019;25:5082–93.
32. van Wilpe S, Sultan S, Gorris MAJ, Somford DM, Kusters-Vandeveldt HVN, Koorstra RHT, et al. Intratumoral T cell depletion following neoadjuvant chemotherapy in patients with muscle-invasive bladder cancer is associated with poor clinical outcome. *Cancer Immunol Immunother* 2023;72:137–49.
33. Leduc C, Adam J, Louvet E, Sourisseau T, Dorvault N, Bernard M, et al. TPF induction chemotherapy increases PD-L1 expression in tumour cells and immune cells in head and neck squamous cell carcinoma. *ESMO Open* 2018;3:e000257.
34. Fukuoka E, Yamashita K, Tanaka T, Sawada R, Sugita Y, Arimoto A, et al. Neoadjuvant chemotherapy increases PD-L1 expression and CD8⁺ tumor-infiltrating lymphocytes in esophageal squamous cell carcinoma. *Anticancer Res* 2019;39:4539–48.
35. Jiménez-Sánchez A, Cybulska P, Mager KL, Koplev S, Cast O, Couturier DL, et al. Unraveling tumor-immune heterogeneity in advanced ovarian cancer uncovers immunogenic effect of chemotherapy. *Nat Genet* 2020;52:582–93.
36. Voorwerk L, Slagter M, Horlings HM, Sikorska K, van de Vijver KK, de Maaker M, et al. Immune induction strategies in metastatic triple-negative breast cancer to enhance the sensitivity to PD-1 blockade: the TONIC trial. *Nat Med* 2019;25:920–8.
37. Linares J, Sallent-Aragay A, Badia-Ramentol J, Recort-Bascuas A, Méndez A, Manero-Rupérez N, et al. Long-term platinum-based drug accumulation in cancer-associated fibroblasts promotes colorectal cancer progression and resistance to therapy. *Nat Commun* 2023;14:746.
38. Baldominos P, Barbera-Mourelle A, Barreiro O, Huang Y, Wight A, Cho J-W, et al. Quiescent cancer cells resist T cell attack by forming an immunosuppressive niche. *Cell* 2022;185:1694–708.e19.
39. Metropulos AE, Munshi HG, Principe DR. The difficulty in translating the preclinical success of combined TGF β and immune checkpoint inhibition to clinical trial. *EBioMedicine* 2022;86:104380.
40. Blanco B, Domínguez-Alonso C, Alvarez-Vallina L. Bispecific immunomodulatory antibodies for cancer immunotherapy. *Clin Cancer Res* 2021;27:5457–64.
41. Ruf P, Bauer HW, Schoberth A, Kellermann C, Lindhofer H. First time intravesically administered trifunctional antibody catumaxomab in patients with recurrent non-muscle invasive bladder cancer indicates high tolerability and local immunological activity. *Cancer Immunol Immunother* 2021;70:2727–35.
42. Sonpavde G, Necchi A, Gupta S, Steinberg GD, Gschwend JE, Van Der Heijden MS, et al. ENERGIZE: a phase III study of neoadjuvant chemotherapy alone or with nivolumab with/without linrodostat mesylate for muscle-invasive bladder cancer. *Future Oncol* 2020;16:4359–68.